www.ietdl.org

Published in IET Microwaves, Antennas & Propagation
Received on 1st June 2012
Revised on 26th September 2012
doi: 10.1049/iet-map.2012.0303

ISSN 1751-8725

Efficiency of arrays composed of high-gain reflector antennas

M. Pasian M. Cametti M. Bozzi L. Perregrini

Department of Electronics, University of Pavia, Pavia, Italy
E-mail: marco.pasian@unipv.it

Abstract: Arrays composed of high-gain reflector antennas are used for radio-astronomical purposes and, more recently, are proposed as ground station for deep space communications. This latter application requires a precise knowledge of the degradation that phase, amplitude and pointing fluctuations impose on the capability of the array to combine coherently the signal received or transmitted from each antenna. In this study, an analytical model for the fluctuation of each parameter (phase, amplitude and pointing) is derived and it is used to predict the efficiency of an array composed of an arbitrary number of high-gain reflector antennas. The analytical models are verified by numerical simulations and applied to an array layout currently proposed as possible future ground stations for the European Space Agency.

1 Introduction

A key parameter of antennas for space application, where faint electromagnetic signals are received from very long distances and a large equivalent isotropic radiated power (EIRP) is required, is the antenna gain. To this aim, reflector antennas are widely adopted because of their large physical area. In particular, the antenna gain can be calculated as [1]

$$G = 4\pi\xi\frac{S}{\lambda^2} \tag{1}$$

where λ is the working wavelength, S is the physical area and ξ is the antenna efficiency, which includes many different terms, such as the illumination efficiency, the spillover efficiency and the surface efficiency. This latter term is one of the principal obstacles that prevents the possibility to build arbitrarily large reflector antennas, as shown in [2]. In fact, beyond a critical mechanical dimension, it is extremely difficult to provide a surface shape close to designed profile (e.g. parabolic reflectors) because of the gravity-induced loads. This in turn poses a practical limit to the maximum gain achievable by a reflector antenna. Currently, the largest fully steerable reflector antennas have main reflector diameters in the order of 100 m [3, 4].

Despite the huge physical area offered by these antennas, the need of even larger collecting areas has led to arrays composed of reflector antennas, which provide an enormous total area while maintaining a reasonable antenna diameter, hence an acceptable surface accuracy. Typical examples of arrays of reflector antennas already operating or under construction are the Very Large Array (VLA), USA [5], the Allen Telescope Array (ATA), USA [6], the Atacama Large Millimeter Array (ALMA), Chile [7] and the Australia Telescope Compact Array (ATCA), Australia [8]. The number of antennas, the diameter of each antenna and the equivalent single-dish diameter for these arrays are reported in Table 1.

All previous arrays have been primarily built and operated for radio-astronomical purposes. Despite the great potential that arrays can offer to deep space (DS) communications, only in some cases they have been applied. Early experiments were performed in the 1970s by the Jet Propulsion Laboratory (JPL). More recently, the arraying capability can be provided at JPL sites by using the 34 m antennas available at each communication complex, normally used as single independent ground stations [9]. However, array are not usually used on a permanent basis and, most of all, they are not considered as the baseline when performing the link budget calculations required to determine the communication systems to be developed and installed on a spacecraft. This is mainly because of the difficulties to achieve a good coherence between the antennas for all operating scenarios (e.g. strong atmospheric turbulence, rains and low elevation angles), a paramount requirement for ground stations, which must usually guarantee a time availability significantly higher than for radio telescopes. Nevertheless, all major space agencies, including National Aeronautics and Space Administration and the European Space Agency (ESA) are funding projects aimed to analyse the feasibility of arrays of reflector antennas specifically devoted to DS communications [10, 11].

For these reasons, it is important to develop analytical tools able to predict the level of coherence achievable for a given array. Mathematical models applicable to normal arrays (i.e. arrays composed of sub-wavelength elements with sub-wavelength reciprocal distances) are described in textbooks and previous works [12, 13]. The development of the arrays

Table 1 Example of arrays of reflector antennas

Array	Number of antennas	Diameter of each antenna, m	Equivalent diameter, m
VLA	27	25	130
ATA	42	6	39
ALMA	64	12	96
ATCA	6	22	54

composed of high-gain antennas for radio-astronomy induced the first studies specifically tailored to this type of arrays [14], whereas only in recent years the attention was focused on arrays for space communications, with theoretical works on phase errors [15, 16], phase and pointing errors [17], phase and amplitude errors [18] and experimental works [19, 20].

However, previous works on arrays composed of high-gain antennas mainly addressed phase errors (possibly adding the effect of amplitude or pointing errors), in some case for a limited number of antennas (two) or with a limited development of general equations to calculate the array performance. Therefore there is a need for a comprehensive and general mathematical model to clearly indicate the effect of phase, amplitude and pointing errors on the array phasing. This paper derives this model, intended to be used as a prediction tool to calculate the performance achievable by an array composed of high-gain antennas separated by multi-wavelength distances, with no limitations on the number of elements composing the array and under different working conditions. This is particularly useful for arrays intended for space communications, where it is very important to know the expected performance also for extreme operating scenario (e.g. severe weather, critical failures). In order to verify the analytical approach, the expected array degradation is also calculated by means of numerical simulation tools for a practical test case, currently proposed as possible future ground station for ESA. The agreement between the numerical simulations and the derived models can be considered as very good.

2 Analytical formulation

The gain of a generic antenna can be expressed by [1]

$$G = 4\pi\frac{K_x}{P} \tag{2}$$

where K_x is the radiation intensity generated along a certain direction and P is the input power. Now, let us consider the standard far-field approximation, which allows for writing

$$\boldsymbol{E}_0 \simeq \hat{\boldsymbol{p}}\sqrt{2\eta_0 K_x}\frac{\mathrm{e}^{-\mathrm{j}2\pi r}}{\lambda} \tag{3}$$

where $\boldsymbol{E}_0$ is the electric field calculated at a distance r from the source, $\hat{\boldsymbol{p}}$ is the polarisation vector and η_0 is the vacuum impedance. Substituting (3) into (2) the antenna gain becomes

$$G \simeq \frac{4\pi}{2\eta_0}\frac{|r\boldsymbol{E}_0|^2}{P} \tag{4}$$

Now, let us consider an array composed of N elements. If high-gain reflector antennas are assumed, any mutual coupling between them can be neglected. Therefore each antenna radiates independently from the others. Equation (4) is accordingly re-formulated as

$$G_{\text{array}} \simeq \frac{4\pi}{2\eta_0}\frac{|r(\boldsymbol{E}_1+\boldsymbol{E}_2+\cdots+\boldsymbol{E}_N)|^2}{P_1+P_2+\cdots+P_N} \tag{5}$$

where $\boldsymbol{E}$ is the electric field generated by the ith antenna and P_i is the input power at the ith antenna. If all antennas have an identical input power P, assuming that the electric fields generated at a distance r are the same (condition of perfect coherence between identical antennas), (5) will become

$$G_{\text{array}} \simeq \frac{4\pi}{2\eta_0}\frac{|rN\boldsymbol{E}|^2}{NP} \simeq N\frac{4\pi}{2\eta_0}\frac{|r\boldsymbol{E}|^2}{P} \simeq NG \tag{6}$$

demonstrating that for an array of high-gain antennas (with no mutual coupling) the maximum gain of the array, achievable if condition of perfect coherence is met, is N times the gain of the single antenna. This approximation is widely adopted in the literature to study this type of arrays [21, 22], which corresponds to the statement that the total collecting area of the array is the sum of the collecting areas given by each antennas.

In order to introduce phase, amplitude and pointing errors, it is useful to express the electric field and the power associated with each antenna as function of a generic excitation coefficient. In fact, the final effect of any phase, amplitude or pointing fluctuations can be thought to be assigned to the excitation coefficient of each antenna. According to this formulation, the following equations hold

$$\boldsymbol{E}_i = C_i\boldsymbol{E}_0 \tag{7}$$

$$C_i = A_i\mathrm{e}^{\mathrm{j}\varphi_i}f(\theta_i) \tag{8}$$

$$P_i = \frac{1}{2}\mathrm{Re}\{Z_0\}|I_0|^2A_i^2 \tag{9}$$

where A_i is the amplitude error (ranging from 1 to 0), φ_i is the phase error, $f(\theta_i)$ is a function accounting for the pointing error, I_0 and Z_0 are the input current and the input impedance of the antenna, respectively. Of course, the power at the input port of each antenna is only affected by A_i. Please note that, for sake of brevity and without loosing generality, the terms A_i, φ_I and $f(\theta_i)$ only account for the excitation errors, and they do not describe the element excitations in absolute values. In other words, the terms intentionally assigned to each element of the array to modify the excitation (e.g. phase terms required to have constructive interference along the pointing direction of the array) are not errors and they are not included in the analysis. Now, substituting (7) and (9) into (5) it is obtained that

$$G_{\text{array}} \simeq \frac{4\pi}{2\eta_0}\frac{2|r\boldsymbol{E}_0(A_1\mathrm{e}^{\mathrm{j}\varphi_1}f(\theta_1)+\cdots+A_N\mathrm{e}^{\mathrm{j}\varphi_N}f(\theta_N))|^2}{\mathrm{Re}\{Z_0\}|I_0|^2(A_1^2+\cdots+A_N^2)} \tag{10}$$

In the next sections, all the different contribution will be addressed.

2.1 Phase errors

The phase errors are best analysed according to a statistical formulation where the mean value and the standard

deviation σ_φ are given as follow

$$\bar{\varphi} = \frac{1}{N}\sum_{i}^{N} \varphi_i \tag{11}$$

$$\sigma_\varphi = \sqrt{\frac{\sum_i^N (\varphi_i - \bar{\varphi})^2}{N}} \tag{12}$$

Assuming that only phase errors are present [which means $A_i = 1$ and $f(\theta_i) = 1$], (10) becomes

$$G_{\text{array}} \simeq \frac{4\pi}{2\eta_0}\frac{2|r\boldsymbol{E}_0(\mathrm{e}^{\mathrm{j}\varphi_1} + \cdots + \mathrm{e}^{\mathrm{j}\varphi_N})|^2}{\mathrm{Re}\{Z_0\}|I_0|^2 N} \tag{13}$$

By dividing (13) for the maximum array gain (i.e. no phase errors, $\varphi_i = 0$) the following equation is derived

$$\frac{G_{\text{array}}}{G_{\text{array}}^{\max}} = \chi_f \simeq \frac{|\mathrm{e}^{\mathrm{j}\varphi_1} + \cdots + \mathrm{e}^{\mathrm{j}\varphi_N}|^2}{N^2} \tag{14}$$

where χ_f is a scalar real number ranging from zero to unity and indicating how good the arraying is. For small phase errors each exponential function in (14) can be approximated by the first three terms of its Taylor series

$$\chi_f \simeq \frac{|1 + \mathrm{j}\varphi_1 - \varphi_1^2/2 + \cdots + 1 + \mathrm{j}\varphi_N - \varphi_N^2/2|^2}{N^2} \tag{15}$$

Thus

$$\chi_f \simeq \frac{\left|N + \mathrm{j}\sum_i^N \varphi_i - (1/2)\sum_i^N (\varphi_i)^2\right|^2}{N^2} = \frac{\left|N + \mathrm{j}N\bar{\varphi} - (1/2)\sum_i^N (\varphi_i)^2\right|^2}{N^2} \tag{16}$$

Now, let us assume a phase fluctuation distribution with mean value equal to zero ($\bar{\varphi} = 0$). This is possible because an arbitrary phase bias can always be added to each term of the distribution to meet this condition, without altering the physical meaning of the phase errors, which is related to relative discrepancies and not to absolute values. In addition, any terms of (16) containing phase errors raised to more than second power can be discarded. This turns into

$$\chi_f \simeq 1 - \sigma_\varphi^2 \tag{17}$$

2.2 Amplitude errors

For amplitude errors, the following statistical parameters can be defined:

$$\bar{A} = \frac{1}{N}\sum_{i}^{N} A_i \tag{18}$$

$$\sigma_A = \sqrt{\frac{\sum_i^N (A_i - \bar{A})^2}{N}} \tag{19}$$

where $\bar{A}$ is the mean value and σ_A is the standard deviation. In order to account for amplitude errors, the terms in (10) are considered accordingly (i.e. $\varphi_i = 0$, $f(\theta_i) = 1$). In addition, as done for phase errors, the array gain is divided by the maximum array gain (i.e. no amplitude errors, $A_i = 1$) to calculate the array degradation

$$\chi_{\text{a}} \simeq \frac{(A_1 + \cdots + A_N)^2}{N(A_1^2 + \cdots + A_N^2)} \tag{20}$$

where χ_{a} is a scalar real number ranging from zero to unity and indicating how good the arraying is. Manipulating (19), (20) can be simplified as

$$\chi_{\text{a}} \simeq \frac{N\bar{A}^2}{A_1^2 + \cdots + A_N^2} \simeq \frac{\sum_i^N A_i^2 - N\sigma_A^2}{\sum_i^N A_i^2} \simeq 1 - \frac{\sigma_A^2}{\bar{P}} \tag{21}$$

where $\bar{P}$ is the mean power reduction suffered by the array

$$\bar{P} = \frac{\sum_i^N A_i^2}{N} \tag{22}$$

From (21) and (22), it is evident the difference with respect to phase errors. In fact, while the periodic nature of the phase allows for considering relative fluctuations and, as a direct consequence, allows for deriving an equation without any information related to the mean value, amplitude errors are strongly related to the absolute value of the excitation coefficients C_i. In other words, the same amplitude fluctuation (i.e. the same standard deviation σ_A) returns different losses according to the mean power reduction. For example, for benign atmospheric conditions the mean power reduction is close to the unity. Therefore a given value for the standard deviation σ_A represents a small percentage variation of the amplitudes. Conversely, for severe weather the mean power reduction can approach very low values (e.g. $\bar{P} < 0.5$) and, in this case, the same standard deviation σ_A represents an higher percentage variation, thus higher losses.

2.3 Pointing errors

For pointing errors, the following statistical parameters can be defined

$$\bar{\theta} = \frac{1}{N}\sum_{i}^{N} \theta_i \tag{23}$$

$$\sigma_\theta^{\text{RMS}} = \sqrt{\frac{\sum_i^N \theta_i^2}{N}} \tag{24}$$

where $\bar{\theta}$ is the mean value and $\sigma_\theta^{\text{RMS}}$ is the root mean square (RMS). Please note that for pointing errors the RMS is more convenient than the standard deviation, which has been defined for phase and amplitude errors. This is easily understood considering the situation where all antennas are affected by equal pointing errors. In this case, the standard deviation would be zero regardless of the magnitude of the pointing error itself, although the RMS assumes different values according to the magnitude of the pointing error. Since it is expected that different pointing errors must be associated with different pointing losses, the RMS is better suited because it allows for maintaining a two-way relationship between pointing errors and pointing losses.

doi: 10.1049/iet-map.2012.0303

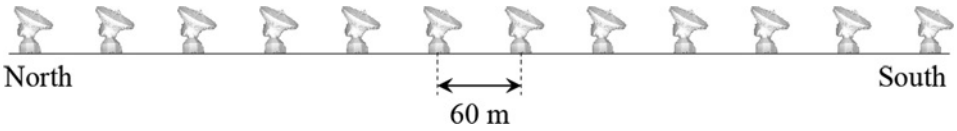

Fig. 1 *Schema of the proposed array layout for the architecture composed of 12 20 m antennas*
Antennas are separated by a reciprocal distance of 60 m and placed along the North–South axis

In order to account for pointing errors, the terms in (10) are considered accordingly (i.e. $\varphi_i = 0$, $A_i = 1$). In addition, as done for phase and amplitude errors, the array gain is divided by the maximum array gain [i.e. no pointing errors, $f(\theta_i) = 1$] to calculate the array degradation

$$\chi_p \simeq \frac{|f(\theta_1) + \cdots + f(\theta_N)|^2}{N^2} \tag{25}$$

where χ_p is a scalar real number ranging from zero to unity and indicating how good the arraying is. For small pointing errors, the typical normalised radiation pattern of a reflector antenna allows for the following approximation [1]

$$f(\theta_i) = 1 - \alpha\theta_i^2 \tag{26}$$

where α is a scalar coefficient. Substituting (26) into (25) and discarding any terms containing pointing errors raised to more than second power the following equation is obtained

$$\chi_p \simeq 1 - 2\alpha(\sigma_\theta^{RMS})^2 \tag{27}$$

3 Test case array configuration

ESA currently runs a worldwide network of reflector antennas in order to provide the appropriate support to different satellites and space probes. In particular, the three 35 m antennas equipped with X-band 20 kW transmitters are devoted to DS missions, such as Rosetta, Mars and Venus Express [23, 24].

For the future, ESA is planning a number of new missions to explore the Solar system that are going to require better performance from the ground segment. In particular, a higher gain over temperature (G/T) is fundamental to achieve very high data rates from inner planets, thus letting huge amount of data to be downloaded (e.g. Mars sample and Return mission). Moreover, a higher G/T is also needed to support a reasonable data rate from Jupiter and Saturn (e.g. the future Jupiter Ganymede Orbiter and the Titan Saturn System Mission). In addition, a higher EIRP is suggested for manned mission to Mars (e.g. Aurora) and to have extra margin in the event of emergency, when only a low-gain antenna may be available on the spacecraft because of a non-correct alignment of the high-gain antenna towards the Earth.

For all these reasons, ESA promoted a detailed feasibility study aimed to address all the aspects related to a possible enhancement of the performance of the current DS antennas, to be achieved by means of an array of reflector antennas [11, 25]. In particular, X band, around 7–8 GHz, is considered as baseline and an array total area around four times the current area provided by a DS antenna is suggested by ESA. In particular, the initial array will operate only in downlink, whereas uplink will remain an option. This is due to the fact that compared to receiving operations, transmission poses more serious problems. In fact, the lack of a reliable closed loop prevents the application of real-time calibrations and adjustments, as normally done for reception [21]. Therefore higher phase, amplitude and pointing errors are expected. Recent experiments succeeded to demonstrate array uplink operations under certain constraints (e.g. short duration, good weather, spacecraft in Earth orbit etc.), but a fully operable uplink array is still ahead [19, 21, 26]. For these reasons, the formulas derived in Section 2, which hold for both downlink and uplink can be used to predict the array response for large phase, amplitude and pointing errors, likely to occur if the array was operated in transmission, providing a useful evaluation tool for the expected uplink performance.

The array configuration selected for the ESA scenario is composed of twelve 20 m antennas [25]. This configuration offer the optimum compromise between the number of antennas and antenna diameter, which means an optimum compromise in terms of sub-arraying, antenna performance, construction cost and budget spread over the years. The array layout, depicted in Fig. 1 was designed to maximise the compactness of the array, a major advantage to reduce the phase and amplitude fluctuations, while avoiding any shadowing for all elevation angles along the ecliptic plane, where almost all DS missions are expected to flight.

4 Numerical validation

In order to verify the analytical formulation derived in Section 2, a numerical simulation of the array described in Section 3 is performed.

In particular, the radiation pattern of the array shown in Fig. 1 is calculated as the sum of the radiated field generated by each antenna, retrieving the maximum array gain. This is possible assuming that no mutual coupling is present between antennas, exactly the same hypothesis already adopted to calculate the equation reported in Section 2 [21, 22]. The radiated field generated by each 20 m antenna is calculated by means of a commercial tool based on physical optics [27]. The parameters of the antenna are reported in Table 2.

In the next paragraphs, phase, amplitude and pointing errors are analysed. Please note that delay errors are not considered because they are negligible if compared with phase errors. This is mainly because of the moderate DS

Table 2 Antenna parameters

Parameter	20 m antenna
configuration	Cassegrain
main reflector diameter, m	20
equivalent f/D	0.27
sub-reflector diameter, m	2.4
sub-reflector eccentricity	1.24
taper angle, degrees	11
taper, dB	−10

service bandwidths with respect to the carrier frequency. In fact, the largest bandwidth for DS services, associated with Delta-differential one-way range (DOR) ranging is equal to around 40 MHz, considerably lower than carrier frequency (around 8 GHz) [28]. To align a 40 MHz channel requires time accuracy significantly better than 25 ns. This is routinely achieved even by large arrays, which can reach a delay error lower then 250 ps [29], that is, 1/100 of the reciprocal of the signal bandwidth, a fraction considered more than adequate to align the time delays [12].

4.1 Phase errors

To simulate phase errors, a Monte Carlo analysis is carried on, assigning a random phase to each antenna excitation and calculating the field radiated by the array by adding the fields radiated from each antenna. This calculation is repeated 3000 times to obtain a good statistical distribution. Please note that the random phase is calculated according to a uniform distribution in order to obtain the same occurrence for all phase combinations, including extreme values that are not likely to occur in the real world. Although in this way the probability for large errors is higher than expected from a real array, this gives the opportunity to extensively test the equations reported in Section 2 also against large phase errors. The same considerations hold for the amplitude and pointing errors, reported in the next paragraphs.

The maximum residual phase error for normal operation when the combiner is locked (downlink) is estimated to be around 7° or even less [25, 29]. However, the phase error can increase up to around 30° for given cases. First, extreme weather condition, with rapid phase variations not compensated in real-time by the correlator, shall be taken into account. Second, when the array is operated for uplink communications closed-loop adjustment techniques are not available or they are less effective and for this reason higher phase fluctuations shall be accounted for [30]. Third, a possible malfunction, or even a complete failure, of the correlator is a critical case worth to be analysed.

The comparison between the analytical formulation, (17), and the numerical simulation is reported in Fig. 2. The agreement can be considered good, with a maximum discrepancy of 0.2–0.3 dB. Moreover, the theoretical curve provides a conservative estimation if compared with the numerical simulation. This is due to the approximation adopted when the Taylor series has been applied and it guarantees a safe margin.

4.2 Amplitude errors

To simulate amplitude errors, a random amplitude is attributed to each antenna excitation. Also in this case, the gain calculation is repeated 3000 times to obtain a good statistical distribution.

According to the RAPIDS and ITU models [31, 32], the power collected by an antenna in X band can be reduced to 50% of the nominal value because of bad atmospheric conditions for a cumulative distribution of 99.99% (i.e. only for a fraction of time equal to 0.01% the power collected by the antenna can be lower than 50%). Assuming as worst case that the power reduction experienced by an antenna is completely un-correlated with the power reduction experienced by another antenna of the array, the maximum power fluctuation among antennas is also set to 50% (i.e. it means that an antenna could receive the incoming signal with no extra losses, whereas another antenna of the array could receive only 50% of the nominal power).

The comparison between the analytical formulation (21) and the numerical simulation is reported in Fig. 3. In particular, three analytical curves are shown, each with a different mean power reduction $\bar{P}$ (1, 0.6 and 0.5). Fig. 3 highlights that, for a given numerical simulation that randomly select all the antenna excitation coefficients A_i (that in turn means a random mean power reduction and a random standard deviation), a top and a bottom limiting curves can be retrieved. The top curve is always associated with a mean power reduction equal to unity. Of course, this is an ideal asymptotic case ($\bar{P} = 1$ means no power reduction at all). The bottom curve depends on the distribution of the numerical simulation. For the case reported in Fig. 3, where the power collected by each antenna can be reduced to 50% of the nominal value, a mean power reduction $\bar{P} = 0.5$ represents the worst case condition (which means all antennas collecting 50% of the nominal power). All other cases (e.g. $\bar{P} = 0.6$) indicates intermediate cases.

Therefore the analytical formulation represents a powerful prediction tool: for a given mean power reduction, which practically means for a given atmospheric condition (e.g. clear sky, light rain etc.), the array gain efficiency G_{ratio} is calculated for any amplitude fluctuation (which depends on the array extension, array working in closed- or open-loop etc.).

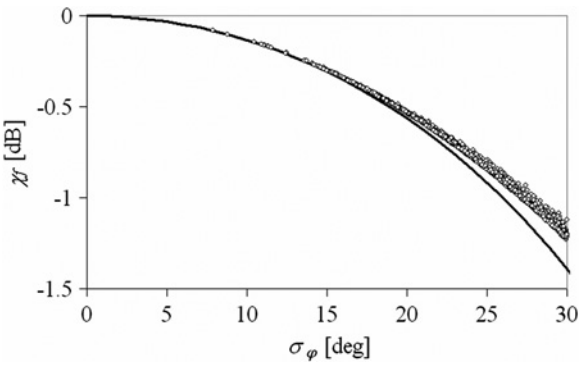

Fig. 2 *Array gain degradation at 8.4 GHz for a given phase standard deviation*

Comparison between analytical formulation (17) (solid black curve) and numerical simulation (white dots)

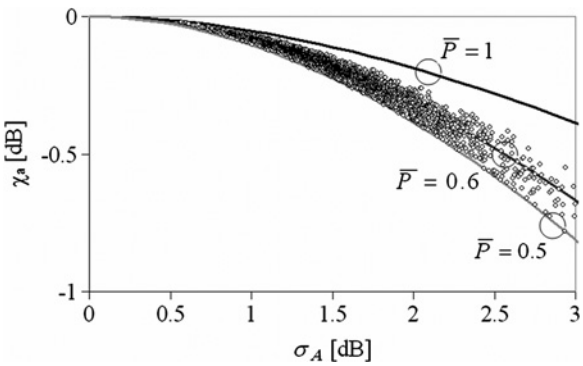

Fig. 3 *Array gain degradation at 8.4 GHz for a given amplitude standard deviation*

Comparison between analytical formulation (21) calculated for different mean power reductions (solid curves) and numerical simulation (white dots)

doi: 10.1049/iet-map.2012.0303

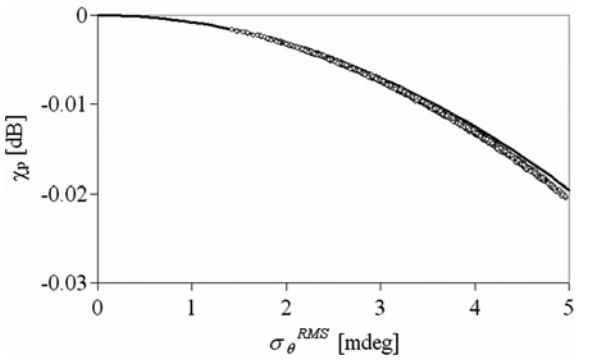

Fig. 4 *Array gain degradation at 8.4 GHz for a given pointing RMS*

Comparison between analytical formulation (27) (solid black curve) and numerical simulation (white dots)

4.3 Pointing errors

To simulate pointing errors, a random pointing is attributed to each antenna excitation. Then, the array radiated field is calculated by adding the radiated field from each antenna. This calculation is repeated 3000 times to obtain a good statistical distribution.

According to Vassallo *et al.* [24], the maximum pointing error for a state-of-the-art 35 m antenna is 5 mdeg for a wind up to 45 km/h with gust of 60 km/h. Other useful comparisons are provided by [5, 8]. In particular, the 25 m antennas of the VLA can achieve a blind pointing of accuracy of around 3 mdeg without wind loads. This value can improve up to 1 mdeg if a reference target (e.g. a pulsar) is available close to the desired direction. The 22 m antennas of the ATCA achieve similar values, both for blind and referenced pointing. Therefore for a 20 m antenna, a maximum pointing errors of 5 mdeg is taken as worst case, including wind loads.

The comparison between the analytical formulation, (27), and the numerical simulation is reported in Fig. 4. The agreement can be considered good, with a slight discrepancy because of the polynomial approximation ($\alpha = 90\ \text{deg}^{-2}$) adopted to represent the 20 m antenna radiation pattern. Please note that the broad beamwidth of a 20 m antenna in X band implies very low de-pointing losses even for a pointing error up to 5 mdeg.

5 Conclusions

This paper presented the mathematical derivation of prediction curves useful to analyse and design arrays composed of many identical reflector antennas. In particular, the array efficiency, that is, the arraying goodness between the elements of the array, is affected by phase, amplitude and pointing fluctuations, mainly because of atmospheric turbulences, failures and mechanical uncertainties. Therefore it is important to have reliable analytical tools to predict the array performance.

Assuming no cross-coupling between antennas, an hypothesis easily met for reflector antennas, this paper calculates the prediction curves for phase, amplitude and pointing fluctuations according to a statistical formulation readily applicable to practical cases, where the required information is usually given in terms of mean values, standard deviations and RMSs.

As validation of the proposed tools, an array specifically designed for the ESA in the frame of a strategic feasibility study is presented. It is composed of 12 20 m antennas and the array radiation pattern is calculated by adding the radiation pattern generated by each antenna, which is turn retrieved from a commercial tool based on physical optics.

The excitation coefficient of each antenna is randomly varied to alternatively include phase, amplitude and pointing errors. The agreement between the theoretical prediction and the numerical simulation can be considered as very good.

6 Acknowledgments

The authors would like to thank Salvador Marti from the European Space Agency, Steve Rawson, Mario Fornaroli and Alan Cloke from Callisto and Paul Maguire from Zelinda for providing the data on the propagation losses and for all useful discussions and hints.

7 References

1 Balanis, C.A.: 'Antenna theory, analysis and design' (John Wiley & Sons, 2005, 3rd edn.)
2 Ruze, J.: 'Antenna tolerance theory – a review', *Proc. IEEE*, 1966, **54**, (4), pp. 633–640
3 Effelsberg telescope official website: http://www.mpifr-bonn.mpg.de/8964/effelsberg, accessed September 2012
4 Green Bank Telescope official website: https://science.nrao.edu/facilities/gbt, accessed September 2012
5 Ulvestad J.S., Perley R.A., Chandler C.J.: 'The very large array observational status summary', 2009
6 Allen Telescope Array official website: http://www.seti.org/ata, accessed September 2012
7 Atacama Large Millimeter Array official website: https://science.nrao.edu/facilities/alma, accessed September 2012
8 Australia Telescope Compact Array official website: http://www.narrabri.atnf.csiro.au/, accessed September 2012
9 Imbriale, W.A.: 'Large antennas of the deep space network' (John Wiley & Sons, 2003)
10 Cesarone, R.J., Abraham, D.S., Deutsch, L.J.: 'Prospects for a next-generation deep-space network', *Proc. IEEE*, 2007, **95**, (10), pp. 1902–1915
11 Marti, S., Bozzi, M., Cametti, M., *et al.*: 'Future architectures for ESA deep space ground station antennas'. European Conf. Antennas and Propagation (EuCAP 2011), Rome, Italy, April 2011
12 Collin, R.E., Zucker, F.J.: 'Antenna theory' (McGraw-Hill, 1969)
13 Elliott, R.: 'Mechanical and electrical tolerances for two-dimensional scanning antenna arrays', *IRE Trans. Antennas Propag.*, 1958, **6**, (1), pp. 114–120
14 Napier, P.J., Thompson, A.R., Ekers, R.D.: 'The very large array: design and performance of a modern synthesis radio telescope', *Proc. IEEE*, 1983, **71**, (11), pp. 1295–1320
15 Sarabandi, K., Wang, F.: 'Phased array of large reflectors for deep-space communication', *IEEE Trans. Aerosp. Electron. Syst.*, 2007, **43**, (1), pp. 251–261
16 D'Addario, L.R.: 'Combining loss of a transmitting array due to phase errors'. IPN Progress Report, 42–175, 2008
17 Stadter, P.A., Kantsiper, B.L., Jablonski, D.G., Golshan, A.R., Costrell, J.: 'Uplink arraying analysis for NASA's deep space network'. 2010 IEEE Aerospace Conf., March 2010
18 Amoozegar, F., Paal, L., Mileant, A., Lee, D.: 'Analysis of errors for uplink array of 34-m antennas for deep space applications'. 2005 IEEE Aerospace Conf., March 2005
19 Morabito, D.D., D'Addario, L.: 'Two-element uplink array loss statistics derived from site test interferometer phase data for the goldstone climate: initial study results'. IPN Progress Report 42–186, 2011
20 Vilnrotter, V., Lee, D., Cornish, T., Tsao, P., Paal, L., Jamnejad, V.: 'Uplink array concept demonstration with the EPOXI spacecraft', *IEEE Aerosp. Electron. Syst. Mag.*, 2010, **25**, (5), pp. 29–35
21 Davarian, F.: 'Uplink arrays for the deep space network', *Proc. IEEE*, 2007, **95**, (10), pp. 1923–1930
22 Rogstad, D.H., Mileant, A., Pham, T.T.: 'Antenna arraying techniques in the deep space network' (John Wiley & Sons, 2003)
23 European Space Agency official website: www.esa.int, accessed September 2012
24 Vassallo, E., Martin, R., Madde, R., *et al.*: 'The European Space Agency's deep-space antennas', *Proc. IEEE*, 2007, **95**, (11), pp. 2111–2131

25 Bozzi, M., Cametti, M., Fornaroli, M., *et al.*: 'Future architectures for European space agency deep space ground stations', *IEEE AP-Mag.*, 2012, **54**, (1), pp. 254–263
26 Davarian, F.: 'Uplink arraying for solar system radar and radio science', *Proc. IEEE*, 2011, **99**, (5), pp. 783–793
27 GRASP9 official website: www.ticra.com, accessed September 2012
28 Madde, R., Morley, T., Lanucara, M., *et al.*: 'A common receiver architecture for ESA radio science and delta-DOR support', *Proc. IEEE*, 2007, **95**, (11), pp. 2215–2223
29 Personal communication with Dr. Jamie Stevens, Senior Systems Scientist at the Australia Telescope Compact Array (ATCA), 25 February 2010
30 Davarian, F.: 'Uplink arraying next steps'. IPN Progress Report 42–175, 2008
31 Rogister, A., Mertens, D., Vanhoenacker-Janvier, D.: 'RAPIDS: RAdio propagation integrated database system'. Meeting and Joint Workshop with COST272, ESTEC, The Netherlands, May 2003
32 Recommendation ITU-R P.618–7, International Telecommunications Union, ITU-R, 2001

doi: 10.1049/iet-map.2012.0303